Synthetic Metals 245 (2018) 151–159

Contents lists available at ScienceDirect

Synthetic Metals

journal homepage: www.elsevier.com/locate/synmet

Enhanced adsorption of cationic and anionic dyes from aqueous solutions by polyacid doped polyaniline

Junjie Shen[a,b,*], Salman Shahid[a,b], Ida Amura[a,b], Adem Sarihan[a,b,c], Mi Tian[a,b], Emma AC Emanuelsson[b,*]

[a] Centre for Advanced Separations Engineering, University of Bath, Bath, BA2 7AY, United Kingdom
[b] Department of Chemical Engineering, University of Bath, Bath, BA2 7AY, United Kingdom
[c] Higher Vocational School, Bilecik Seyh Edebali University, Bilecik, 11210, Turkey

ARTICLE INFO

Keywords:
Polyaniline
Dye adsorption
Polyacid
Doping
Methylene blue
Rose bengal

ABSTRACT

A new high surface area polyaniline (PANI) adsorbent was synthesized by matrix polymerization of aniline in the presence of a polyacid, poly(2-acrylamido-2-methyl-1-propanesulfonic acid) (PAMPSA). Morphological and physicochemical properties of PANI-PAMPSA were characterized by field emission scanning electron microscope (FESEM), Fourier transform infrared spectroscopy (FTIR), X-ray powder diffraction (XRD), nitrogen adsorption/desorption and zeta potential measurement. Adsorption properties were evaluated using methylene blue (MB) and rose bengal (RB) as model dyes.

The results showed that PANI-PAMPSA obtained a well-defined porous structure with a specific surface area ($126\ m^2\ g^{-1}$) over 10 times larger than that of the emeraldine base PANI (PANI-EB) ($12\ m^2\ g^{-1}$). The maximum adsorption capacities were $466.5\ mg\ g^{-1}$ for MB and $440.0\ mg\ g^{-1}$ for RB, higher than any other PANI-based materials reported in the literature. The FTIR analysis and zeta potential measurement revealed that the adsorption mechanisms involved π-π interaction and electrostatic interaction. The adsorption kinetics were best described by a pseudo-second-order model, and the adsorption isotherms followed the Langmuir model. The thermodynamic study indicated that the adsorption was a spontaneous endothermic process. Overall, the convenient synthesis and the high adsorption capacity make PANI-PAMPSA a promising adsorbent material for dye removal.

1. Introduction

Synthetic organic dyes from wastewater of textile, paper, plastic, cosmetics, pharmaceutical and food industries are a major source of environmental contamination [1,2]. It is estimated that 5000 tons of dyes are discharged into the environment every year [3]. These dyes impart color to water which not only damages the aesthetic nature of water, but also interferes with the transmission of sunlight and thus disturbs the biological metabolism processes of aquatic communities [4,5]. More importantly, most of the dyes have serious harmful effects on human beings, which span from skin and eye irritation to dysfunction of brain, liver, kidney and reproductive system [1]. Due to the low biodegradability of dyes, the conventional biological methods are not effective in treating dye effluents [1]. A wide range of physicochemical techniques has been employed to remove dyes, such as adsorption [2], coagulation [6], membrane filtration [7], oxidation [8], electrochemical destruction [9] and photochemical degradation [10]. Among these techniques, adsorption has attracted great attention because of its easy operation, low cost, and high efficiency [1]. Numerous types of adsorbents, such as activated carbon, zeolite, alumina, silica, biomaterials, and polymers have been extensively used for dye removal [2,11].

Polyaniline (PANI) is one of the most studied conducting polymers due to its ease of synthesis, low cost, environmentally stability and the unique doping/dedoping property [12]. The emeraldine base PANI (PANI-EB) and the emeraldine salt PANI (PANI-ES) can be efficiently switched to each other by doping (protonation) and dedoping (deprotonation), respectively [13,14]. The utilization of PANI as a potential

Abbreviations: PANI, polyaniline; PAMPSA, poly(2-acrylamido-2-methyl-1-propanesulfonic acid; MB, methylene blue; RB, rose bengal; CV, crystal violet; MO, methyl orange; PR, procion red; OG, orange G; CBB, coomassie brilliant blue; RBBR, remazol brilliant blue R; AG, alizarine cyanine green; MG, malachite green; CR, Congo red; TMP, tin (II) molybdophosphate; ZSP, zirconium (IV) silicophosphate; PTSA, *p*-toluenesulfonic acid; CSA, camphorsulfonic acid

* Corresponding authors at: Department of Chemical Engineering, University of Bath, Bath, BA2 7AY, United Kingdom.
E-mail addresses: J.Shen@bath.ac.uk (J. Shen), E.A.Emanuelsson-Patterson@bath.ac.uk (E.A. Emanuelsson).

https://doi.org/10.1016/j.synthmet.2018.08.015
Received 20 June 2018; Received in revised form 19 August 2018; Accepted 23 August 2018
Available online 05 September 2018
0379-6779/

Table 1
A selective summary of adsorption capacities of PANI-based materials for dye removal.

Material	Dye	Maximum adsorption capacity (mg g^{-1})	Reference
PANI-EB			
PANI nanoparticle	MB	6.1	[19]
PANI nanotube	MB	9.2	[20]
PANI nanotube/silica composite	MB	10.3	[21]
Nanostructured crosslinked PANI	MB	13.8	[22]
Nanoporous hypercrosslinked PANI	CV, MO	245, 220	[23]
PANI-ES			
PANI-HCl	PR	18.4	[15]
PANI-HCl	MO	154.6	[24]
PANI-HCl	MB	192.3	[25]
PANI-HCl	OG, CBB, RBBR, AG	175, 129, 100, 56	[26]
PANI-HCl/chitosan composite	OG, CBB, RBBR	322, 357, 303	[27]
PANI-HCl/TMP nanocomposite	MG	78.9	[28]
PANI-HCl/ZSP nanocomposite	MB	12	[29]
PANI-H_2SO_4	MO	75.9	[30]
PANI-phytic acid hydrogel	MB	71.2	[31]
PANI-PTSA	OG, CBB, RBBR, AG	342, 207, 171, 95	[32]
PANI-CSA	OG, CBB, RBBR, AG	400, 231, 254, 151	[32]
PANI-CSA/polyamide 6 composite	MO	81.9	[33]
PANI-PAMPSA	MB, RB	466.5, 440.0	This study

adsorbent for dye removal is due to two reasons: (1) its large amount of amine and imine functional groups are expected to interact with organic compounds [12]; (2) the charge transfer induced by doping enables PANI to interact with ionic species via electrostatic interaction [15]. There are several excellent reviews in the literature discussing the applications of PANI-based materials for the removal of dyes from wastewater/aqueous solutions, and the reader is referred in particular to those by Zare and coworkers [16], and Huang and coworkers [12]. A selective summary of adsorption capacities of PANI-based materials is provided in Table 1. Although PANI is widely used for dye removal, there are two main challenges restricting its actual performance. Firstly, the bare PANI-EB particles can easily aggregate because of the inter- and intramolecular interactions, which significantly reduces the surface area and hence results in lower adsorption capacities [12]. Secondly, PANI doped by small molecule acid is prone to dedoping because the small molecule acid evaporates easily at room temperature [17,18], which will reduce the surface charge of PANI and therefore affect the electrostatic interaction between PANI and dye.

The present work aims to overcome these challenges by doping PANI with a polyacid, namely poly(2-acrylamido-2-methyl-1-propanesulfonic acid) (PAMPSA). PAMPSA is a strong polyacid distinguished by flexible polymer backbone and short distances between sulfonic groups of neighbouring repeat units [34]. PAMPSA offers many advantages compared to small molecule acids: (1) PAMPSA can easily adapt its conformation to match the spatial distribution of nitrogen sites in PANI and form a double-strand structure [34,35]. The double-strand structure confers a higher stability than the single-strand structure formed between small molecule acid and PANI [36]; (2) PAMPSA is not volatile and will not cause dedoping; (3) PAMPSA brings large amount of sulfonic, carbonyl and amide functional groups into PANI, which may improve the processability and create more adsorption sites. Our previous research found that PAMPSA as a dopant can improve the porosity and chemical stability of PANI membranes for organic solvent nanofiltration [37]. However, to the best of our knowledge, there has been no study about PAMPSA doped PANI (PANI-PAMPSA), or any polyacid doped PANI, as adsorbents for dye removal.

Hence, the objective of the present work was to investigate the adsorption properties of PANI-PAMPSA towards a cationic dye (methylene blue, MB) and an anionic dye (rose bengal, RB). The experimental variables affecting optimal adsorption were evaluated. The kinetics, isotherms, thermodynamics, and mechanisms of adsorption were elucidated in detail.

2. Materials and methods

2.1. Chemicals

Analytical grade MB, RB, aniline, ammonium persulfate (APS), hydrochloric acid (HCl), N-methyl-2-pyrrolidone (NMP), 4-methyl piperidine (4MP) were obtained from Sigma-Aldrich, UK. The structure and chemical properties of MB and RB are summarized in Table S1. PAMPSA (MW 800,000 g mol^{-1}) was supplied by Fisher Scientific, UK. Deionized (DI) water was produced by an ELGA deionizer from PURELAB Option, USA.

2.2. Synthesis

PANI-PAMPSA was synthesized by matrix (template) polymerization. This approach uses polyacid as a template to promote the 'head-to-tail' coupling of aniline along the chain of the polyacid macromolecule, leading to the formation of a well-defined molecular structure of PANI [38–40]. Specifically, 18.23 mL (0.2 mol) of aniline, at 4:1 monomer to acid repeat unit molar ratio, was dissolved in 200 mL of 0.1 M PAMPSA solution. The polymerization of aniline was initiated by the slow addition of 128 mL of 1.56 M APS solution using a peristaltic pump at a speed of 20 mL h^{-1} at 15 °C. The mixture was left for 24 h under stirring for full polymerization. The final solution was filtered and the obtained PANI-PAMPSA was rinsed with DI water to remove unreacted chemicals, and then washed with acetone to remove oligomers. To prepare PANI-EB, 18.23 mL (0.2 mol) of aniline was dissolved in 200 mL of 1 M HCl solution. The polymerization process was similar to PANI-PAMPSA, but the powder obtained was stirred in 33.3% (w/v) ammonia solution for 4 h to deprotonate the emeraldine salt. The obtained PANI-EB was then rinsed with DI water to remove excess ammonia and then washed with acetone to remove oligomers. Both PANI-PAMPSA and PANI-EB were dried in a vacuum oven at 60 °C for 24 h, and then ground using mortar and pestle. The final color of PANI-PAMPSA was dark green, and the final color of PANI-EB was purple bronze.

2.3. Characterization

The morphological and physiochemical properties of PANI-PAMPSA were characterized in comparison to PANI-EB. Morphology of the samples was studied by a JEOL 6301 F field emission scanning electron microscope (FESEM). Fourier transform infrared (FTIR) spectra were obtained by a PerkinElmer Spectrum 100 ATR-FTIR spectrometer. Each

FTIR spectrum had 32 scans with 4 cm^{-1} resolution. The X-ray powder diffraction (XRD) patterns were obtained with a Bruker AXS D8 Advance X-ray diffractometer, equipped with a Vantec-1 detector using Cu Kα radiation source (λ = 1.5418 Å). The specific surface areas were obtained from low pressure (up to 1 bar) nitrogen sorption measurements at 77 K using a Micromeritics 3Flex volumetric gas sorption analysis system. The specific surface area was calculated according to the British Standard guidelines for the BET method [41] from regression analysis of data in the relative pressure range from 0.05 to 0.3, using the manufacturer-recommended equilibration period, equating to a 2 min soak time. The surface charge was determined by the zeta potential measurement. Specifically, 10 mg of PANI-EB or PANI-PAMPSA was added in 20 mL of DI water to make a 0.5 g L^{-1} dispersion. The pH of the dispersion was varied between 3 and 12 by the addition of 1 mM HCl or 1 mM NaOH solution. The zeta potential of the dispersion was measured by a Malvern Nano ZS ZetaSizer with folded capillary zeta cells (DTS1070).

2.4. Dye adsorption experiments

The adsorption of dyes onto PANI adsorbents were carried out in batch adsorption experiments. Typically, a certain amount of PANI-EB or PANI-PAMPSA was added into 20 mL of dye solution at 25 °C and 300 rpm stirring condition. At regular intervals, 1 mL of the suspension was withdrawn and centrifugated at 4000 rpm by a Thermo Scientific Medifuge centrifuge, and the concentration of the respective dye in the supernatant was measured by a Agilent Cary 100 UV–vis spectrophotometer. The concentrations of RB and MB were calibrated by Beer-Lambert law at λ_{max} values of 549 and 663 nm, respectively.

The experimental variables affecting adsorption, including contact time, adsorbent dosage, initial dye concentration and solution pH, were evaluated. To determine the effect of adsorbent dosage as well as the initial dye concentration, a series of experiments were carried out by varying the adsorbent dosage from 0.1 to 0.8 g L^{-1}, and the initial dye concentration from 25 to 200 mg L^{-1}. To investigate the influence of solution pH on adsorption capacity, the pH of the dye solution was adjusted from 3 to 12 before adsorption, by using 1 mM HCl or 1 mM NaOH solution. The adsorption kinetic, isotherm, and thermodynamic parameters were determined to characterize the adsorption process. For the adsorption kinetic, isotherm and thermodynamic experiments, the solution pH was fixed at pH = 7 and the adsorbent dosage was 0.5 g L^{-1}. After the adsorption reached equilibrium, the dye-loaded adsorbents were separated by centrifugation, washed with DI water, and dried at 80 °C for 24 h. Possible adsorption mechanisms were investigated by FTIR analysis.

All of the experiments were done in triplicate and the average values of the results were used for data analysis. The adsorption capacity and the percentage removal were calculated using Eqs. (1) and (2) where q_t is the adsorbed amount of dye at time t (mg g^{-1}); c_0 and c_t are the initial and present dye concentrations (mg L^{-1}); V is the solution volume (L); and m is the mass of PANI (g).

$$q_t = \frac{(c_0 - c_t)V}{m} \quad (1)$$

$$Removal = \frac{c_0 - c_t}{c_0} \times 100\% \quad (2)$$

3. Results and discussion

3.1. Characterization of PANI-EB and PANI-PAMPSA

FESEM images of PANI-EB and PANI-PAMPSA are shown in Fig. 1. It can be observed that the structure of PANI-EB is tightly packed, making it difficult to distinguish the size and shape of individual particles (Fig. 1(a)). This is in agreement with previous literature which reported that PANI-EB tends to aggregate during the polymerization process [42]. In comparison, the structure of PANI-PAMPSA is composed of porous particle aggregates (Fig. 1(b)). The FESEM image of PANI-PAMPSA at 150k magnification shows that the average diameter of the particles is in the range of 50 and 100 nm (Fig. S1). The porous structure of PANI-PAMPSA is expected to provide a larger surface area and thus increase the dye adsorption in comparison to PANI-EB.

Fig. 2(a) shows the FTIR spectra of PANI-EB and PANI-PAMPSA. The typical bands of PANI-EB are observed at 1586 cm^{-1} (quinoid C═C stretching), 1490 cm^{-1} (benzenoid C═C stretching), 1378 cm^{-1} (quinoid C—N stretching), 1286 cm^{-1} (aromatic amine C—N stretching), 1156 cm^{-1} (aromatic imine C═N stretching) and 818 cm^{-1} (C—H bending) [43]. The bands of PANI-PAMPSA at approximately 1641 cm^{-1} and 1032 cm^{-1} are attributed to the C═O stretching and the symmetric O═S═O stretching, which correspond to the carbonyl and sulfonic groups of PAMPSA, respectively [34]. It is noticeable that the bands of quinoid (1586 cm^{-1}) and benzenoid (1490 cm^{-1}) in PANI-EB show a red shift to 1546 cm^{-1} and 1440 cm^{-1} in the spectrum of PANI-PAMPSA. This proves the interaction between the backbone of PANI and PAMPSA, which is associated with the π-electron delocalization induced by protonation [18]. The bands at 1296 cm^{-1} and 1148 cm^{-1} are assigned to the protonated amine and protonated imine groups, respectively. The FTIR results suggest that the incorporation of PAMPSA in PANI is through an interaction between sulfonic groups of PAMPSA and nitrogen atoms of PANI [34].

Fig. 2(b) shows the XRD patterns of PANI-EB and PANI-PAMPSA. The crystalline phases of PANI-EB can be identified by some blunt peaks at 2θ values of 15.6°, 20.1° and 24.2°. The peaks at 20.1° and 24.2° represent the reflection plane of (020) and (200) [44], corresponding to the periodicity parallel and perpendicular to the polymer chain of PANI, respectively [45]. As reported in literatures, most regions in the PANI structure are amorphous [46]. When PAMPSA was doped into PANI, the XRD pattern shows two peaks at 14.2° and 25.5°, which may indicate the rearrangement in the polymer chain of PANI due to the interaction with the PAMPSA macromolecule [34]. The number and intensity of peaks in PANI-PAMPSA are both lower than that in PANI-EB, representing a decrease in crystallinity. Given that PAMPSA is an amorphous polymer, the incorporation of large amounts of PAMPSA would make ordering of PANI chains difficult. The less-ordered structures of acid doped PANI in comparison to PANI-EB has previously been reported [42,46].

Fig. 2(c) displays the nitrogen physisorption (adsorption/desorption) isotherms for PANI-EB and PANI-PAMPSA. The specific surface areas of the adsorbents can be calculated from the physisorption isotherms using the BET theory. PANI-EB had a specific surface area of 12 $m^2 g^{-1}$, while PANI-PAMPSA had a higher specific surface area of 126 $m^2 g^{-1}$. As reported in the literature, PANI-EB with various morphologies obtained significantly different specific surface areas, including conventional PANI-EB (< 20 $m^2 g^{-1}$) [47], nanostructured PANI-EB (24–80 $m^2 g^{-1}$) [48,49], and crosslinked PANI-EB (349–1083 $m^2 g^{-1}$) [22,23]. Nevertheless, the specific surface area of PANI-PAMPSA has never been reported. This study shows that the polyacid doping leads to a 10-fold increase in the specific surface area of PANI-EB, which concurs with results of FESEM images in Fig. 1. This is possibly because the PANI particles are located along the PAMPSA macromolecule to form the double-strand structure during polymerization [34]. In the absence of PAMPSA, PANI-EB particles are susceptible to aggregation and hence, larger particles with smaller specific surface areas are formed.

Fig. 2(d) illustrates the variations of zeta potential of PANI-EB and PANI-PAMPSA in the pH range 3–12. PANI-EB exhibits negative zeta potential at all pH values because it became dedoped by the alkaline treatment. The zeta potential of PANI-PAMPSA also remains negative at all pH values, and its absolute value increases from 16.5 mV (at pH = 3) to 34.6 mV (at pH = 12). When in an acidic environment, PANI-PAMPSA is in the doped form where the backbone carries positive

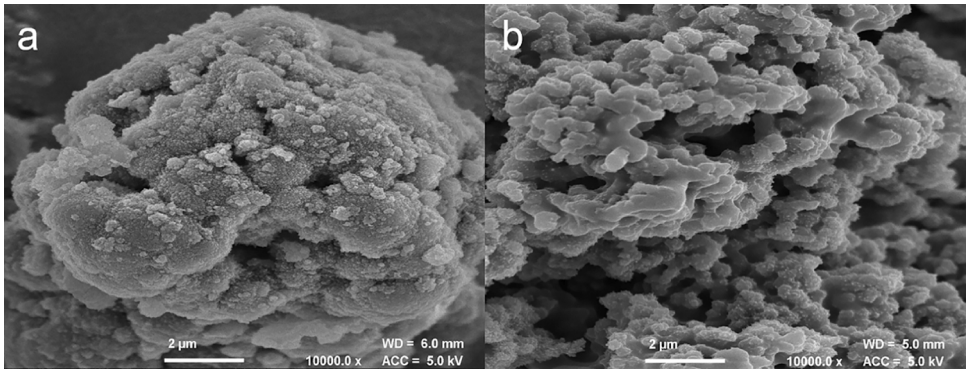

Fig. 1. FESEM images of (a) PANI-EB and (b) PANI-PAMPSA.

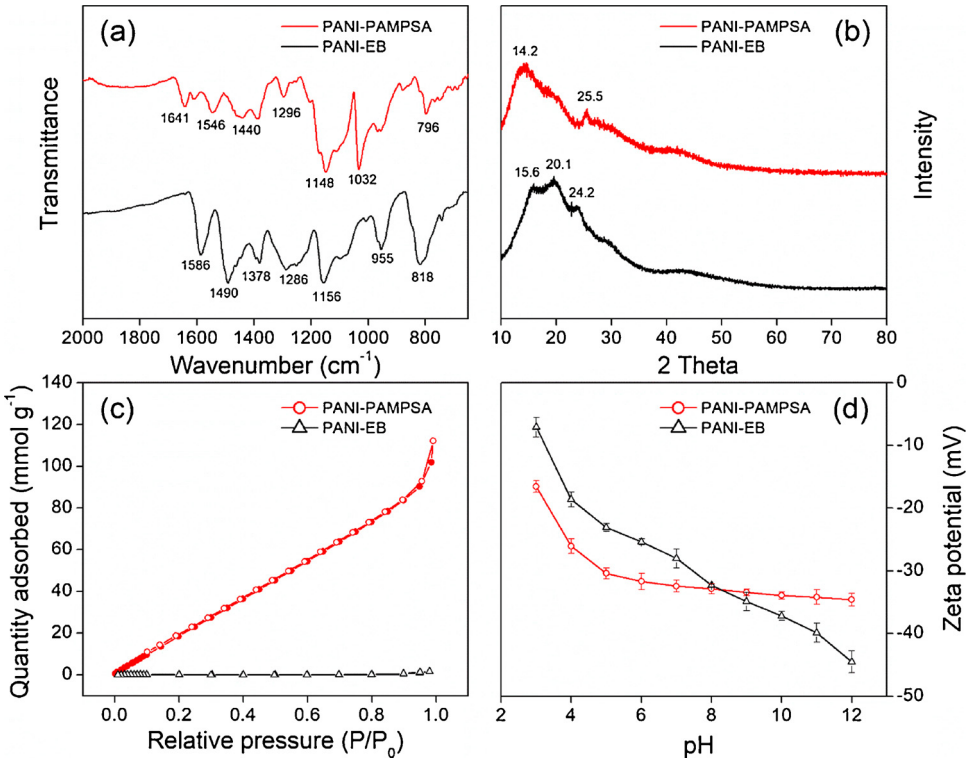

Fig. 2. (a) FTIR; (b) XRD; (c) N_2 sorption isotherms and (d) zeta potential of PANI-EB and PANI-PAMPSA.

charge [50]. However, the polymer matrix on the whole is negatively charged due to the dissociation of the PAMPSA macromolecule (pKa = 0.87). This is similar to the findings by Mukherjee, Sharma, Saini and De [51] who found that PANI doped with an anionic surfactant, dodecyl benzene sulfonic acid (DBSA), remained negatively charged from pH 2 to 12. With the increase of the solution pH, the positive sites in PANI-PAMPSA get deprotonated, and the net surface charge becomes more negative. It should be noted that PANI-PAMPSA shows a more gradual increase in the absolute value of zeta potential compared to PANI-EB. This is because the functional groups from PAMPSA, such as $-SO_3H$ and $-COOH$ groups, have buffer effects against pH variations [52]. The zeta potential of PANI-PAMPSA is always below −30 mV between pH 5 and 12, which suggests a stable colloidal system that is resistant to particle aggregation and is therefore beneficial to adsorption [53].

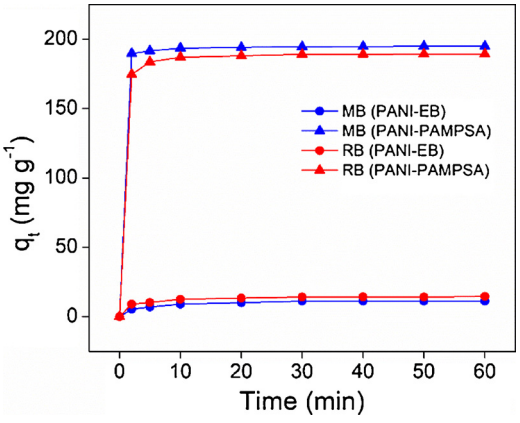

Fig. 3. Effect of contact time on adsorption capacity of PANI-EB and PANI-PAMPSA for MB and RB (0.5 g L^{-1} adsorbent, 100 mg L^{-1} dye, pH = 7, 25 °C).

3.2. Adsorption capacities of PANI-EB and PANI-PAMPSA

The adsorption capacity curves of PANI-EB and PANI-PAMPSA for MB and RB at different time intervals are shown in Fig. 3. The

adsorption process is extremely rapid in the initial 2 min, especially for PANI-PAMPSA. All the curves become flat after 10 min, indicating the adsorption equilibrium is reached. PANI-EB shows relatively low adsorption capacities for MB (11.2 mg g^{-1}) and RB (14.5 mg g^{-1}), which are likely attributed to the particle aggregation and the small specific surface area. Compared to PANI-EB, PANI-PAMPSA possesses much higher adsorption capacities for both MB and RB. The adsorption capacity of PANI-PAMPSA for MB is 194.9 mg g^{-1}, which is significantly higher than any other PANI-based materials, such as nanostructured PANI-EB (4.8 mg g^{-1}) [20], crosslinked PANI-EB (6.9 mg g^{-1}) [22], and PANI-nickel ferrite nanocomposite (6.6 mg g^{-1}) [54]. The adsorption capacity of PANI-PAMPSA for RB is 189.4 mg g^{-1}. Although adsorption of RB by PANI-based materials has not been explored previously, the result from this study is in general consistent with the above-mentioned adsorption capacities of PANI-based materials for other anionic dyes [26,32]. Another interesting finding is that the equilibrium time of PANI-PAMPSA (approximately 10 min) is much faster than previous studies that report equilibrium times in the range of 60–120 min [20,23,55], which is an additional advantage for PANI-PAMPSA. These results demonstrate that PANI-PAMPSA can be utilized as a very efficient adsorbent to remove both cationic and anionic dyes from aqueous solutions.

3.3. Effect of adsorbent dosage, initial dye concentration and solution pH

To observe the effect of adsorbent dosage on dye adsorption, 100 mg L^{-1} of MB or RB at pH = 7, 25 °C was put in contact with various amounts of PANI-PAMPSA (0.1–0.8 g L^{-1}). As can be seen in Eq. (1), the adsorption capacity and the adsorbent dosage have an inverse relationship. Fig. 4(a) shows that when the amount of PANI-PAMPSA increases, the adsorption capacities for both dyes decrease. This is because the adsorption sites available will not be fully utilized at a higher adsorbent dosage in comparison to a lower adsorbent dosage [23,56]. Maximum adsorption capacities for MB and RB are 525.2 and 412.7 mg g^{-1} with PANI-PAMPSA dosage of 0.1 g L^{-1}. When it comes to the percentage removal, 95% removal of both dyes can be achieved with PANI-PAMPSA dosage of 0.5 g L^{-1}. Therefore, 0.5 g L^{-1} was chosen as the fixed dosage of PANI-PAMPSA for subsequent experiments.

The effect of initial dye concentration on the adsorption capacity of PANI-PAMPSA is shown in Fig. 4(b). The adsorption capacities for MB and RB increase almost linearly with the initial dye concentration in the range of 25–200 mg L^{-1}. This can be explained by the increase in the adsorbate to adsorbent ratio [23]. Previous studies found that the initial dye concentration is the main driving force for mass transfer from solution to the adsorbent [2,55,57]. The higher the initial dye concentration, the greater the driving force for adsorption, causing stronger interactions between dye molecules and available sites on the adsorbent surface [55]. The reduce of linearity for RB at higher dye concentrations may suggest a nearly saturation limit for PANI-PAMPSA [23]. A moderate initial dye concentration of 100 mg L^{-1} was chosen as the fixed adsorbate concentration for further study.

The solution pH plays a key role in the adsorption process, because it affects the surface charge and active sites of the adsorbent, as well as the speciation of the adsorbate [56,58]. At low pH, both MB and RB are neutral. When the pH increases, MB becomes positively charged (pKa = 3.8), and RB becomes negatively charged (pKa = 4.7) [59,60]. Fig. 2(d) shows that the negative surface charge of PANI-PAMPSA increases from pH 3 to pH 12, which means the stronger electrostatic interaction (attractive for MB and repulsive for RB) is at higher side of pH. Fig. 4(c) plots the adsorption capacities of PANI-PAMPSA for MB and RB as a function of solution pH. As expected from the zeta potential result, the adsorption capacity for MB gradually increases from 139.3 to 205.8 mg g^{-1}, and that for RB decreases from 210.9 to 134.6 mg g^{-1} with an increase of pH from 3 to 12. Such opposite trends in ionic dyes has been previously reported [23].

3.4. Adsorption kinetics, isotherms and thermodynamics

The adsorption kinetics is an important characteristic that provides information in regards to the controlling mechanisms of the adsorption process. The kinetics data were fitted into three kinetics models:

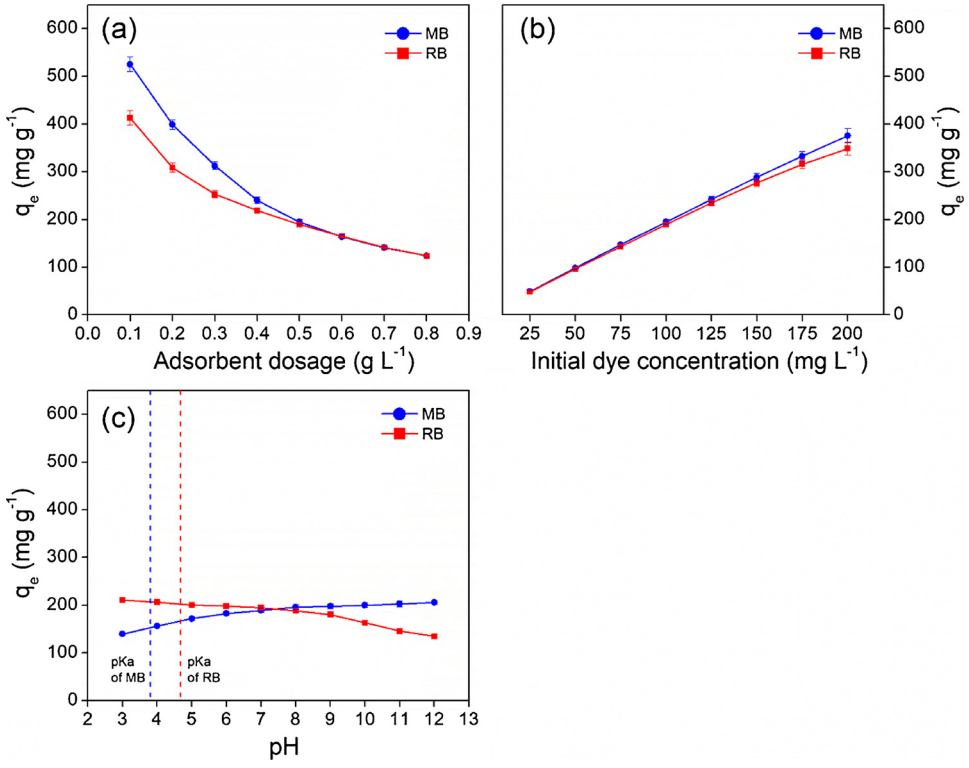

Fig. 4. Effect of (a) adsorbent dosage; (b) initial dye concentration; (c) solution pH on adsorption capacity of PANI-PAMPSA for MB and RB.

pseudo-first-order (PFO) [61], pseudo-second-order (PSO) [62], and intraparticle diffusion (IPD) [63] models. The PFO and PSO models assume that the reaction at the liquid/solid interface is the limiting mechanism, while the IPD model assumes that the reaction is a very rapid process and the adsorption is controlled by intraparticle diffusion [64,65]. The PFO, PSO and IPD models are expressed as Eqs. (3)–(5), respectively. q_t and q_e are the adsorption capacity (mg g^{-1}) of PANI-PAMPSA at time t and at equilibrium, k_1 is the PFO rate constant (min^{-1}), k_2 is the PSO rate constant (g mg^{-1} min^{-1}), k_d is the IPD rate constant (mg g^{-1} $min^{-0.5}$), and C is a constant indicating the thickness of the boundary layer. Non-linear forms of PFO and PSO equations are used as they are found to be more suitable than the linear forms to determine the kinetic parameters [66,67].

$$q_t = q_e(1-e^{-k_1 t}) \tag{3}$$

$$q_t = \frac{k_2 q_e^2 t}{1 + k_2 q_e t} \tag{4}$$

$$q_t = k_d t^{0.5} + C \tag{5}$$

The comparison of PSO and PFO models for adsorption of MB and RB respectively by PANI-PAMPSA are shown in Fig. 5(a) and (b), and the corresponding kinetic parameters and the correlation coefficient (R^2) are summarized in Table S2. The PSO model shows a better fit for both MB and RB than the PFO model based on the R^2 values, and the calculated q_e value agrees very well with the experimental value. Therefore, the adsorption kinetics of MB and RB onto PANI-PAMPSA can be satisfactorily described by the PSO model. Such a finding is in good agreement with previous studies [22–24,32,55,68].

The possibility of intraparticle diffusion is explored by using the IPD model in Fig. 5(c). If the plot of q_t versus $t^{0.5}$ gives a straight line that passes through the origin of coordinates, then the adsorption process is controlled by intraparticle diffusion only [69]. However, the data exhibit multi-linear plots and the straight lines deviate from the origin. The first straight line depicts the intraparticle diffusion of dye molecules in macropores of PANI-PAMPSA, and the second straight line represents the diffusion in micropores [69,70]. The result reveals that intraparticle diffusion is not the controlling mechanism in the adsorption system.

The adsorption isotherms can be used to describe the equilibrium relationship between the adsorbent and the adsorbate at a constant temperature, and is thus important for optimization of the adsorption system. In this study, the adsorption isotherm data were fitted using the Langmuir [71] and the Freundlich [72] models. The Langmuir model describes monolayer adsorption at a homogeneous surface, while the Freundlich model describes multilayer adsorption on a heterogeneous system.

The non-linear form of the Langmuir model can be represented by Eq. (6) where q_m is the maximum adsorption capacity of the adsorbent (mg g^{-1}), and K_L is the Langmuir constant which is related to the energy of adsorption (L mg^{-1}).

$$q_e = \frac{K_L q_m C_e}{1 + K_L C_e} \tag{6}$$

The separation factor (R_L) of the Langmuir isotherm can be defined by Eq. (7). The value of R_L reveals the adsorption nature which can be either irreversible ($R_L = 0$), favourable ($0 < R_L < 1$), linear ($R_L = 1$), or unfavourable ($R_L > 1$) [73].

$$R_L = \frac{1}{1 + K_L c_0} \tag{7}$$

The non-linear form of the Freundlich model can be expressed as Eq. (8) where K_F is the Freundlich constant ($mg^{1-(1/n)}$ $L^{1/n}$ g^{-1}), and n is the index number indicating the extent of adsorption.

$$q_e = K_F C_e^{1/n} \tag{8}$$

The adsorption isotherms of MB and RB onto PANI-PAMPSA are shown in Fig. 6 and the parameters obtained are given in Table S3. It can be observed that the Langmuir model provides a better fit to the experimental data in comparison to the Freundlich model. The values of R^2 of the Langmuir model are closer to 1, showing that the Langmuir model explains the adsorption process of both dyes better than the

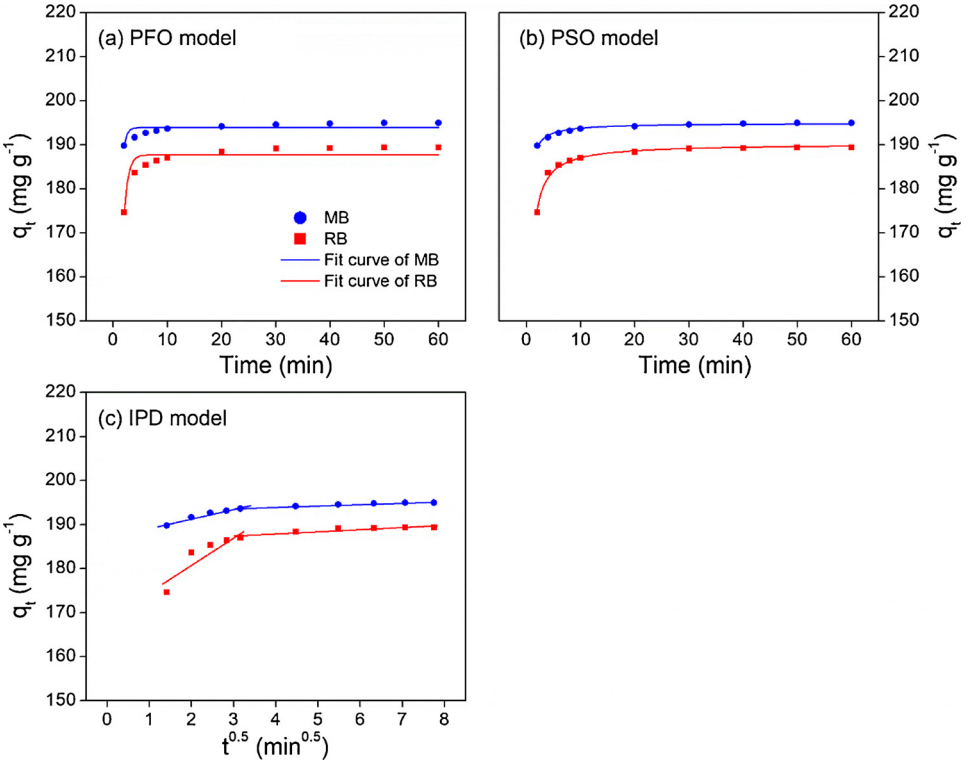

Fig. 5. Adsorption kinetics of RB and MB onto PANI-PAMPSA fitted by (a) PFO, (b) PSO, and (c) IPD models (0.5 g L^{-1} adsorbent, 100 mg L^{-1} dye, pH = 7, 25 °C).

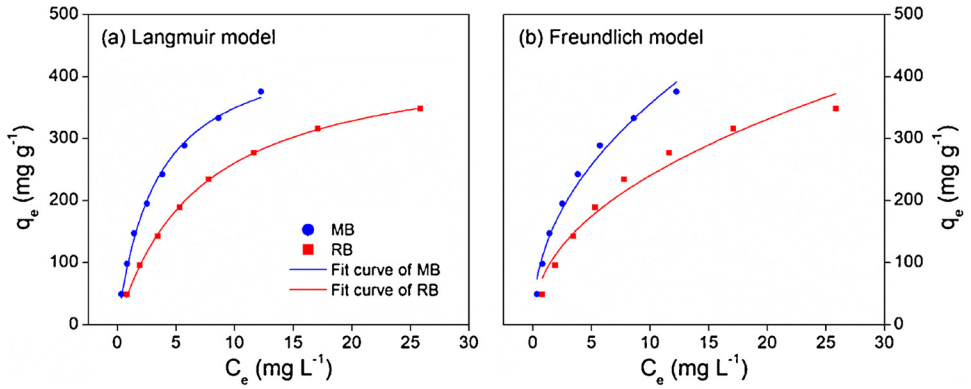

Fig. 6. Adsorption isotherms of RB and MB onto PANI-PAMPSA fitted by (a) Langmuir and (b) Freundlich models (0.5 g L^{-1} adsorbent, pH = 7, 25 °C).

Freundlich model. This suggests that the adsorption of dyes on PANI-PAMPSA follows a monolayer coverage adsorption mechanism [23,74]. Fig. S2 shows the variation of R_L with the initial dye concentration. The R_L value lies between 0.01 and 0.12 for MB, and between 0.03 and 0.22 for RB. This demonstrates the favourable adsorption of both dyes onto PANI-PAMPSA. The maximum adsorption capacities of PANI-PAMPSA based on the Langmuir model are 466.5 mg g^{-1} for MB, and 440.0 mg g^{-1} for RB, when the adsorbent dose is 0.5 g L^{-1} and the temperature is 25 °C. To our knowledge, PANI-PAMPSA has higher adsorption capacities than any other PANI-based materials (Table 1), and is among the most effective adsorbents for dye removal (such as commercial activated carbon and chitosan) [1,2].

To investigate whether the adsorption process is spontaneous or not, four sets of adsorption experiments were conducted at various temperatures from 298 to 318 K. The thermodynamic parameters are calculated as per Eq. (9) and Eq. (10), where $\Delta G°$ is the standard free energy change (kJ mol^{-1}), T is the temperature (K), R is the universal gas constant (8.314 J mol^{-1} K^{-1}), K_0 is the adsorption equilibrium constant, $\Delta H°$ is the standard enthalpy change (kJ mol^{-1}), and $\Delta S°$ is the standard entropy change (kJ mol^{-1} K^{-1}). K_0 was determined by plotting $\ln(q_e/c_e)$ versus c_e at different temperatures and extrapolating c_e to zero [75]. The values of $\Delta H°$ and $\Delta S°$ were calculated from the slope and intercept of the plot of $\ln K_0$ versus $1/T$, respectively.

$$\Delta G° = -RT \ln K_0 \tag{9}$$

$$\ln K_0 = \frac{\Delta S°}{R} - \frac{\Delta H°}{RT} \tag{10}$$

The values of the thermodynamic parameters are given in Table 2. The negative values of $\Delta G°$ measured at all temperatures indicate that the adsorption process is thermodynamically spontaneous [76]. With an increase in temperature, the absolute value of $\Delta G°$ increases gradually, implying that the adsorption process is more favourable at higher temperature. The positive values of $\Delta H°$ confirm the endothermic nature of the adsorption process [77]. The positive values of $\Delta S°$ imply an increase in the randomness at the adsorbent and adsorbate interface [78], which reflects a good affinity of the PANI-PAMPSA surface towards dye molecules. Additionally, the type of adsorption (physisorption and chemisorption) can be classified to a certain extent by the thermodynamic parameters. Generally, $\Delta G°$ for physisorption is between −20 and 0 kJ mol^{-1}, and for chemisorption is between −80 and −400 kJ mol^{-1} [79]. $\Delta H°$ due to physisorption is less than 84 kJ mol^{-1}, while $\Delta H°$ due to chemisorption takes value between 84 and 420 kJ mol^{-1} [80]. Therefore, the values of $\Delta G°$ and $\Delta H°$ in Table 2 both suggest that adsorption of dyes onto PANI-PAMPSA was driven by a physisorption process.

Table 2
Thermodynamic parameters of dye adsorption onto PANI-PAMPSA (0.5 g L^{-1} adsorbent, pH = 7).

Dye	$\Delta G°$ (kJ mol^{-1})				$\Delta H°$ (kJ mol^{-1})	$\Delta S°$ (kJ mol^{-1} K^{-1})
	298 K	308 K	318 K	328 K		
MB	−11.89	−12.52	−13.28	−14.12	10.31	0.07
RB	−9.82	−10.49	−11.16	−11.73	9.20	0.06

3.5. Adsorption mechanisms

The adsorption of organic dyes on PANI-based materials in general follows mechanisms such as π-π interaction, electrostatic interaction, and hydrogen bonding [19,23,24]. As mentioned above, the adsorption of MB and RB follows the monolayer coverage mechanism, which rules out the possibility of hydrogen bonding because intermolecular hydrogen bonding between dye molecules would cause multilayer adsorption [74,81]. At pH = 3 when the dyes are neutral and the electrostatic interaction between dye and PANI-PAMPSA is shielded, the adsorption capacities are still pretty high (139.3 mg g^{-1} for MB and 210.9 mg g^{-1} for RB). This suggests that the most possible driving force for the adsorption of dyes is the π-π interaction between aromatic rings of PANI-PAMPSA and dye molecules [74,82]. On the other hand, as shown in Fig. 4(c), at pH = 12 when the electrostatic interaction (attractive for MB and repulsive for RB) and π-π interaction coexist, the adsorption capacity for MB is increased by 48%, and that for RB is decreased by 36%, in comparison to those at pH = 3. This evidences that electrostatic interaction also plays an important role in the adsorption of ionic dyes.

In order to prove the adsorption mechanisms, the FTIR spectra of PANI-PAMPSA before and after dye adsorption were compared (Fig. 7). The nitrogen atom of PANI interacts with the sulfonic groups of PAMPSA and this causes more delocalization (two vibrational bands of C–N stretching of secondary aromatic amine [34]). In the MB-loaded PANI-PAMPSA, these peaks overlap with the intense vibrational bands of C—N stretching and CH_3 stretching of the dye, making it difficult to determine the nature of the interaction. The bands due to S═O stretching shift from 1153 – 1034 to 1109 – 1025 cm^{-1} and this is possibly due to electron delocalization caused by electrostatic interaction between MB and PANI-PAMPSA [23]. In the RB-loaded PANI-PAMPSA, the vibrational band due to the quinoid C═C stretching of PANI-PAMPSA shifts from 1546 to 1563 cm^{-1}, which is due to π-π interaction between the localized π electrons in the aromatic rings of PANI-PAMPSA and RB. Therefore, the main adsorption mechanism of PANI-PAMPSA towards both cationic and anionic dyes is π-π interaction while electrostatic interaction has an additional attractive and repulsive effect on the cationic and anionic dyes, respectively.

4. Conclusions

In this study, a polyacid doped PANI adsorbent PANI-PAMPSA was

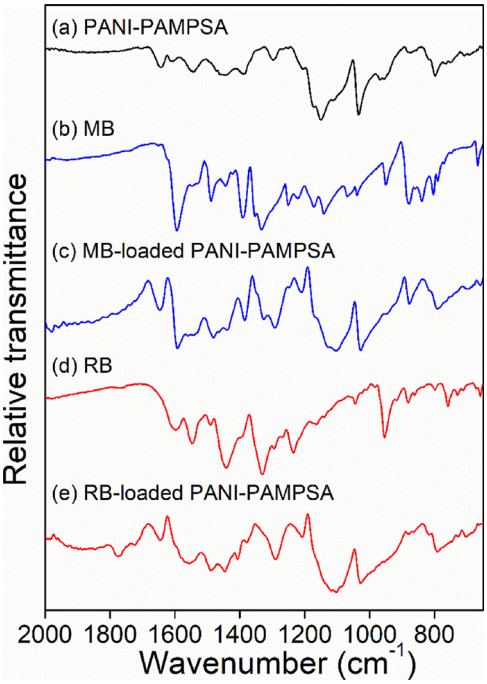

Fig. 7. FTIR of spectra of (a) PANI-PAMPSA, (b) MB, (c) MB-loaded PANI-PAMPSA, (d) RB, and (e) RB-loaded PANI-PAMPSA.

used for dye removal for the first time. PANI-PAMPSA was synthesized by matrix polymerization of aniline in the presence of the polyacid PAMPSA. FTIR and XRD results evidenced the successful incorporation of PAMPSA in PANI. FESEM and BET analysis showed that PAMPSA was of great importance for the formation of the porous structure of PANI-PAMPSA, which had a specific surface area of 126 $m^2 g^{-1}$. Adsorption experiments showed that PANI-PAMPSA could substantially remove both cationic (MB) and anionic (RB) dyes from the aqueous solution, while PANI-EB was not effective for dye adsorption. The adsorption capacities of PANI-PAMPSA were significantly influenced by the adsorbent dosage, the initial dye concentration, and the solution pH. The adsorption kinetics obeyed the PSO model, and the isotherms followed the Langmuir monolayer model. Based on the Langmuir isotherm, the maximum adsorption capacities of PANI-PAMPSA were 466.5 mg g^{-1} and 440.0 mg g^{-1} for MB and RB, respectively. These values were significantly higher than other previously reported PANI-based materials. The thermodynamic parameters suggested that the adsorption process was spontaneous and endothermic in nature. The adsorption mechanisms included π-π interaction and electrostatic interaction between the dyes and the adsorbent. For large-scale applications, this adsorbent can be used in a combined adsorption-filtration process, or be used as adsorptive membranes. This work not only presented a promising PANI adsorbent for organic dyes, but also shed some light on the development of other conducting polymer-based adsorbents for wastewater treatment.

Acknowledgements

This work was supported by the European Research Council (ERC) Consolidator Grant TUNEMEM (Project reference: 646769; funded under H2020-EU.1.1.-EXCELLENT SCIENCE). The authors thank Dr. Gabriele Kociok-Köhn and Dr. Philip Fletcher (University of Bath) for XRD and FESEM analysis, and the technician team at the Department of Chemical Engineering, University of Bath for technical support.

Appendix A. Supplementary data

Supplementary material related to this article can be found, in the online version, at doi:https://doi.org/10.1016/j.synthmet.2018.08.015.

References

[1] V.K. Gupta, Suhas, Application of low-cost adsorbents for dye removal—a review, J. Environ. Manage. 90 (2009) 2313–2342.
[2] M.T. Yagub, T.K. Sen, S. Afroze, H.M. Ang, Dye and its removal from aqueous solution by adsorption: a review, Adv. Colloid Interface Sci. 209 (2014) 172–184.
[3] A. Pirkarami, M.E. Olya, Removal of dye from industrial wastewater with an emphasis on improving economic efficiency and degradation mechanism, J. Saudi Chem. Soc. 21 (2017) S179–S186.
[4] G.E. Walsh, L.H. Bahner, W.B. Horning, Toxicity of textile mill effluents to freshwater and estuarine algae, crustaceans and fishes, Environ. Pollut. A 21 (1980) 169–179.
[5] W.G. Kuo, Decolorizing dye wastewater with Fenton's reagent, Water Res. 26 (1992) 881–886.
[6] S.Sadri Moghaddam, M.R.Alavi Moghaddam, M. Arami, Coagulation/flocculation process for dye removal using sludge from water treatment plant: optimization through response surface methodology, J. Hazard. Mater. 175 (2010) 651–657.
[7] S. Yu, M. Liu, M. Ma, M. Qi, Z. Lü, C. Gao, Impacts of membrane properties on reactive dye removal from dye/salt mixtures by asymmetric cellulose acetate and composite polyamide nanofiltration membranes, J. Membr. Sci. 350 (2010) 83–91.
[8] S. Wang, A comparative study of Fenton and Fenton-like reaction kinetics in decolourisation of wastewater, Dyes Pigm. 76 (2008) 714–720.
[9] Ö. Gerçel, Removal of textile dye from aqueous solution by electrochemical method, Sep. Sci. Technol. 51 (2016) 711–717.
[10] V.K. Gupta, R. Jain, A. Mittal, M. Mathur, S. Sikarwar, Photochemical degradation of the hazardous dye Safranin-T using TiO2 catalyst, J. Colloid Interface Sci. 309 (2007) 464–469.
[11] A. Kausar, M. Iqbal, A. Javed, K. Aftab, Z.-i.-H. Nazli, H.N. Bhatti, S. Nouren, Dyes adsorption using clay and modified clay: a review, J. Mol. Liq. 256 (2018) 395–407.
[12] Y. Huang, J. Li, X. Chen, X. Wang, Applications of conjugated polymer based composites in wastewater purification, RSC Adv. 4 (2014) 62160–62178.
[13] M. Wan, J. Yang, Mechanism of proton doping in polyaniline, J. Appl. Polym. Sci. 55 (1995) 399–405.
[14] D.W. Hatchett, M. Josowicz, J. Janata, Acid doping of polyaniline: spectroscopic and electrochemical studies, J. Phys. Chem. B 103 (1999) 10992–10998.
[15] A.N. Chowdhury, S.R. Jesmeen, M.M. Hossain, Removal of dyes from water by conducting polymeric adsorbent, Polym. Adv. Technol. 15 (2004) 633–638.
[16] E.N. Zare, A. Motahari, M. Sillanpää, Nanoadsorbents based on conducting polymer nanocomposites with main focus on polyaniline and its derivatives for removal of heavy metal ions/dyes: a review, Environ. Res. 162 (2018) 173–195.
[17] Y. Moo Lee, S. Yong Nam, S. Yong Ha, Pervaporation of water/isopropanol mixtures through polyaniline membranes doped with poly(acrylic acid), J. Membr. Sci. 159 (1999) 41–46.
[18] L. Xu, Electrically Tuneable Membranes: Revolutionising Separation and Fouling Control for Membrane Reactors, Department of Chemical Engineering, University of Bath, UK, 2016.
[19] M. Ayad, G. El-Hefnawy, S. Zaghlol, Facile synthesis of polyaniline nanoparticles; its adsorption behavior, Chem. Eng. J. 217 (2013) 460–465.
[20] M.M. Ayad, A.A. El-Nasr, Adsorption of cationic dye (Methylene Blue) from water using polyaniline nanotubes base, J. Phys. Chem. C 114 (2010) 14377–14383.
[21] M.M. Ayad, A. Abu El-Nasr, J. Stejskal, Kinetics and isotherm studies of methylene blue adsorption onto polyaniline nanotubes base/silica composite, J. Ind. Eng. Chem. 18 (2012) 1964–1969.
[22] M. Ayad, S. Zaghlol, Nanostructured crosslinked polyaniline with high surface area: synthesis, characterization and adsorption for organic dye, Chem. Eng. J. 204–206 (2012) 79–86.
[23] V. Sharma, P. Rekha, P. Mohanty, Nanoporous hypercrosslinked polyaniline: an efficient adsorbent for the adsorptive removal of cationic and anionic dyes, J. Mol. Liq. 222 (2016) 1091–1100.
[24] L. Ai, J. Jiang, R. Zhang, Uniform polyaniline microspheres: a novel adsorbent for dye removal from aqueous solution, Synth. Met. 160 (2010) 762–767.
[25] S. Agarwal, I. Tyagi, V.K. Gupta, F. Golbaz, A.N. Golikand, O. Moradi, Synthesis and characteristics of polyaniline/zirconium oxide conductive nanocomposite for dye adsorption application, J. Mol. Liq. 218 (2016) 494–498.
[26] D. Mahanta, G. Madras, S. Radhakrishnan, S. Patil, Adsorption of sulfonated dyes by polyaniline emeraldine salt and its kinetics, J. Phys. Chem. B 112 (2008) 10153–10157.
[27] V. Janaki, B.-T. Oh, K. Shanthi, K.-J. Lee, A.K. Ramasamy, S. Kamala-Kannan, Polyaniline/chitosan composite: an eco-friendly polymer for enhanced removal of dyes from aqueous solution, Synth. Met. 162 (2012) 974–980.
[28] P. Gharbani, Synthesis of polyaniline-tin(II)molybdophosphate nanocomposite and application of it in the removal of dyes from aqueous solutions, J. Mol. Liq. 242 (2017) 229–234.
[29] V.K. Gupta, D. Pathania, N.C. Kothiyal, G. Sharma, Polyaniline zirconium (IV) silicophosphate nanocomposite for remediation of methylene blue dye from waste water, J. Mol. Liq. 190 (2014) 139–145.
[30] M. Tanzifi, S.H. Hosseini, A.D. Kiadehi, M. Olazar, K. Karimipour, R. Rezaiemehr, I. Ali, Artificial neural network optimization for methyl orange adsorption onto polyaniline nano-adsorbent: kinetic, isotherm and thermodynamic studies, J. Mol. Liq. 244 (2017) 189–200.
[31] B. Yan, Z. Chen, L. Cai, Z. Chen, J. Fu, Q. Xu, Fabrication of polyaniline hydrogel:

synthesis, characterization and adsorption of methylene blue, Appl. Surf. Sci. 356 (2015) 39–47.
[32] D. Mahanta, G. Madras, S. Radhakrishnan, S. Patil, Adsorption and desorption kinetics of anionic dyes on doped polyaniline, J. Phys. Chem. B 113 (2009) 2293–2299.
[33] Y. Xia, T. Li, J. Chen, C. Cai, Polyaniline (skin)/polyamide 6 (core) composite fiber: preparation, characterization and application as a dye adsorbent, Synth. Met. 175 (2013) 163–169.
[34] O.L. Gribkova, A.A. Nekrasov, M. Trchova, V.F. Ivanov, V.I. Sazikov, A.B. Razova, V.A. Tverskoy, A.V. Vannikov, Chemical synthesis of polyaniline in the presence of poly(amidosulfonic acids) with different rigidity of the polymer chain, Polymer 52 (2011) 2474–2484.
[35] M.A. Guseva, A.A. Isakova, O.L. Gribkova, V.A. Tverskoi, V.F. Ivanov, A.V. Vannikov, Y.A. Fedotov, Matrix polymerization of aniline in the presence of polyamides containing sulfo acid groups, Polym. Sci. A 49 (2007) 4–11.
[36] J.-W. Jeon, Y. Ma, J.F. Mike, L. Shao, P.B. Balbuena, J.L. Lutkenhaus, Oxidatively stable polyaniline:polyacid electrodes for electrochemical energy storage, PCCP 15 (2013) 9654–9662.
[37] J. Shen, S. Shahid, A. Sarihan, D.A. Patterson, E.A.C. Emanuelsson, Effect of polyacid dopants on the performance of polyaniline membranes in organic solvent nanofiltration, Sep. Purif. Technol. 204 (2018) 336–344.
[38] V.F. Ivanov, O.L. Gribkova, K.V. Cheberyako, A.A. Nekrasov, V.A. Tverskoi, A.V. Vannikov, Template synthesis of polyaniline in the presence of poly-(2-acrylamido-2-methyl-1-propanesulfonic acid), Russ. J. Electrochem. 40 (2004) 299–304.
[39] S. Bhadra, D. Khastgir, N.K. Singha, J.H. Lee, Progress in preparation, processing and applications of polyaniline, Prog. Polym. Sci. 34 (2009) 783–810.
[40] Z.A. Boeva, V.G. Sergeyev, Polyaniline: synthesis, properties, and application, Polym. Sci. C 56 (2014) 144–153.
[41] British Standards Institution, Determination of the Specific Surface Area of Powders-Part 1: BET Method of Gas Adsorption for Solids (Including Porous Materials), (1996).
[42] M.A.C. Mazzeu, L.K. Faria, Ad.M. Cardoso, A.M. Gama, M.R. Baldan, E.S. Gonçalves, Structural and morphological characteristics of polyaniline synthesized in pilot scale, J. Aerosp. Technol. Manage. 9 (2017) 39–47.
[43] J. Jang, J. Ha, J. Cho, Fabrication of water-dispersible polyaniline-poly(4-styrenesulfonate) nanoparticles for inkjet-printed chemical-sensor applications, Adv. Mater. 19 (2007) 1772–1775.
[44] Z.-J. Gu, Q. Shen, Synthesis, characterization and comparison of polyaniline 1D-structure controlled by poly(l-lactide) and poly(d-lactide), Superlattices Microstruct. 89 (2016) 53–58.
[45] L. Shi, X. Wang, L. Lu, X. Yang, X. Wu, Preparation of TiO2/polyaniline nanocomposite from a lyotropic liquid crystalline solution, Synth. Met. 159 (2009) 2525–2529.
[46] Zeghioud Hichem, Lamouri Saad, Safidine Zitouni, B. Mohammed, Chemical synthesis and characterization of highly soluble conducting polyaniline in the mixtures of common solvents, J. Serb. Chem. Soc. 80 (2015) 917–931.
[47] K. Zarrini, A.A. Rahimi, F. Alihosseini, H. Fashandi, Highly efficient dye adsorbent based on polyaniline-coated nylon-6 nanofibers, J. Clean. Prod. 142 (2017) 3645–3654.
[48] M. Trchová, E.N. Konyushenko, J. Stejskal, J. Kovářová, G. Ćirić-Marjanović, The conversion of polyaniline nanotubes to nitrogen-containing carbon nanotubes and their comparison with multi-walled carbon nanotubes, Polym. Degrad. Stab. 94 (2009) 929–938.
[49] J. Du, Z. Liu, B. Han, Z. Li, J. Zhang, Y. Huang, One-pot synthesis of the macroporous polyaniline microspheres and Ag/polyaniline core-shell particles, Microporous Mesoporous Mater. 84 (2005) 254–260.
[50] Y. Wang, X.N. Guan, C.-Y. Wu, M.-T. Chen, H.-H. Hsieh, H.D. Tran, S.-C. Huang, R.B. Kaner, Processable colloidal dispersions of polyaniline-based copolymers for transparent electrodes, Polym. Chem. 4 (2013) 4814–4820.
[51] R. Mukherjee, R. Sharma, P. Saini, S. De, Nanostructured polyaniline incorporated ultrafiltration membrane for desalination of brackish water, Environ. Sci.: Water Res. Technol. 1 (2015) 893–904.
[52] H. Cui, Y. Qian, H. An, C. Sun, J. Zhai, Q. Li, Electrochemical removal of fluoride from water by PAOA-modified carbon felt electrodes in a continuous flow reactor, Water Res. 46 (2012) 3943–3950.
[53] O. Duman, S. Tunç, Electrokinetic and rheological properties of Na-bentonite in some electrolyte solutions, Microporous Mesoporous Mater. 117 (2009) 331–338.
[54] M.R. Patil, V.S. Shrivastava, Adsorptive removal of methylene blue from aqueous solution by polyaniline-nickel ferrite nanocomposite: a kinetic approach, Desalin. Water Treat. 57 (2016) 5879–5887.
[55] B.N. Patra, D. Majhi, Removal of anionic dyes from water by potash alum doped polyaniline: investigation of kinetics and thermodynamic parameters of adsorption, J. Phys. Chem. B 119 (2015) 8154–8164.
[56] J. Shen, M.F. Evangelista, G. Mkongo, H. Wen, R. Langford, G. Rosair, M.R.S. McCoustra, V. Arrighi, Efficient defluoridation of water by Monetite nanorods, Adsorption 24 (2018) 135–145.
[57] Y. Bulut, H. Aydın, A kinetics and thermodynamics study of methylene blue adsorption on wheat shells, Desalination 194 (2006) 259–267.
[58] C. Sairam Sundaram, N. Viswanathan, S. Meenakshi, Defluoridation chemistry of synthetic hydroxyapatite at nano scale: equilibrium and kinetic studies, J. Hazard. Mater. 155 (2008) 206–215.
[59] X. He, K.B. Male, P.N. Nesterenko, D. Brabazon, B. Paull, J.H.T. Luong, Adsorption and desorption of Methylene Blue on porous carbon monoliths and nanocrystalline cellulose, ACS Appl. Mater. Interfaces 5 (2013) 8796–8804.
[60] R.W. Sabnis, Handbook of Biological Dyes and Stains: Synthesis and Industrial Applications, John Wiley & Sons, Inc., USA, 2010.
[61] S. Lagergren, About the theory of so-called adsorption of soluble substances, Kungliga Svenska Vetenskapsakademiens Handlingar 24 (1898) 1–39.
[62] Y.S. Ho, G. McKay, Pseudo-second order model for sorption processes, Process Biochem. 34 (1999) 451–465.
[63] W.J. Weber, J.C. Morris, Kinetics of adsorption on carbon from solutions, J. Sanit. Eng. Div. 89 (1963) 31–60.
[64] J.-P. Simonin, On the comparison of pseudo-first order and pseudo-second order rate laws in the modeling of adsorption kinetics, Chem. Eng. J. 300 (2016) 254–263.
[65] F.-C. Wu, R.-L. Tseng, R.-S. Juang, Initial behavior of intraparticle diffusion model used in the description of adsorption kinetics, Chem. Eng. J. 153 (2009) 1–8.
[66] K.V. Kumar, Linear and non-linear regression analysis for the sorption kinetics of methylene blue onto activated carbon, J. Hazard. Mater. 137 (2006) 1538–1544.
[67] J. Lin, L. Wang, Comparison between linear and non-linear forms of pseudo-first-order and pseudo-second-order adsorption kinetic models for the removal of methylene blue by activated carbon, Front. Environ. Sci. Eng. Chin. 3 (2009) 320–324.
[68] M.H. Mohamed, A. Dolatkhah, T. Aboumourad, L. Dehabadi, L.D. Wilson, Investigation of templated and supported polyaniline adsorbent materials, RSC Adv. 5 (2015) 6976–6984.
[69] V. Fierro, V. Torné-Fernández, D. Montané, A. Celzard, Adsorption of phenol onto activated carbons having different textural and surface properties, Microporous Mesoporous Mater. 111 (2008) 276–284.
[70] A. Witek-Krowiak, Analysis of influence of process conditions on kinetics of malachite green biosorption onto beech sawdust, Chem. Eng. J. 171 (2011) 976–985.
[71] I. Langmuir, The adsorption of gases on plane surfaces of glass, mica and platinum, J. Am. Chem. Soc. 40 (1918) 1361–1403.
[72] C.-h Yang, Statistical mechanical study on the Freundlich isotherm equation, J. Colloid Interface Sci. 208 (1998) 379–387.
[73] T.W. Weber, R.K. Chakravorti, Pore and solid diffusion models for fixed-bed adsorbers, AlChE J. 20 (1974) 228–238.
[74] J. Xiao, W. Lv, Z. Xie, Y. Tan, Y. Song, Q. Zheng, Environmentally friendly reduced graphene oxide as a broad-spectrum adsorbent for anionic and cationic dyes via π–π interactions, J. Mater. Chem. A 4 (2016) 12126–12135.
[75] A.A. Khan, R.P. Singh, Adsorption thermodynamics of carbofuran on Sn (IV) arsenosilicate in H+, Na+ and Ca2+ forms, Colloids Surf. 24 (1987) 33–42.
[76] Y.-H. Li, Z. Di, J. Ding, D. Wu, Z. Luan, Y. Zhu, Adsorption thermodynamic, kinetic and desorption studies of Pb2+ on carbon nanotubes, Water Res. 39 (2005) 605–609.
[77] H. Gao, T. Kan, S. Zhao, Y. Qian, X. Cheng, W. Wu, X. Wang, L. Zheng, Removal of anionic azo dyes from aqueous solution by functional ionic liquid cross-linked polymer, J. Hazard. Mater. 261 (2013) 83–90.
[78] M. Ghaedi, B. Sadeghian, A.A. Pebdani, R. Sahraei, A. Daneshfar, C. Duran, Kinetics, thermodynamics and equilibrium evaluation of direct yellow 12 removal by adsorption onto silver nanoparticles loaded activated carbon, Chem. Eng. J. 187 (2012) 133–141.
[79] C.-Y. Kuo, C.-H. Wu, J.-Y. Wu, Adsorption of direct dyes from aqueous solutions by carbon nanotubes: determination of equilibrium, kinetics and thermodynamics parameters, J. Colloid Interface Sci. 327 (2008) 308–315.
[80] R. Ahmad, R. Kumar, Adsorptive removal of congo red dye from aqueous solution using bael shell carbon, Appl. Surf. Sci. 257 (2010) 1628–1633.
[81] H. Kim, S.-O. Kang, S. Park, H.S. Park, Adsorption isotherms and kinetics of cationic and anionic dyes on three-dimensional reduced graphene oxide macrostructure, J. Ind. Eng. Chem. 21 (2015) 1191–1196.
[82] C.R. Minitha, M. Lalitha, Y.L. Jeyachandran, L. Senthilkumar, R.T. Rajendra Kumar, Adsorption behaviour of reduced graphene oxide towards cationic and anionic dyes: co-action of electrostatic and π – π interactions, Mater. Chem. Phys. 194 (2017) 243–252.